Romanian Reports in Physics, Vol. 64, No. 1, P. 64–80, 2012

PROTON CAPTURE CROSS SECTIONS MEASUREMENTS ON N = 82 NUCLEI ^{139}La AND ^{141}Pr

I. PRECUP[1*], C. BADITA[1*], E. DRAGULESCU[1*], M. PETRE[1*], M. DIMA[1*], C. PETRE[2*]

[1]"Horia Hulubei" National Institute of Nuclear Physics and Engineering, PO BOX MG-6, Bucharest 077125, Romania, E-mail author 4: petre_m@yahoo.com
[2] University of Bucharest, Bucharest, Romania

Received February 2, 2011

Abstract. The proton-capture reactions ^{139}La (p,γ) ^{140}Ce and ^{141}Pr (p,γ) ^{142}Nd have been investigated at energies E_P = 2–5 MeV via a low-background spectrometer based on a 4π NaI(Tl) summing detectors. Cross sections have been calculated by means of the statistical model code NON SMOKER.

Key words: low-background, cross section, proton-capture.

1. INTRODUCTION

Explosive nuclear burning in the astrophysical environments produces unstable nuclei, which again can be targets for subsequent reactions. In addition, it involves a very large number of stable nuclei, which are not fully explored by experiments. Thus is it necessary to be able to predict reaction cross sections and thermonuclear rates with the aid of theoretical models. Explosive burning in supernovae involves, in general, intermediate mass and heavy nuclei. Due to a large nucleon number they have intrinsically a high density of excited states. A high level density in the compound nucleus at the appropriate excitation energy allows one to make use of statistical model approach for compound nuclear reactions which averages over resonances.

It is often termed that the statistical model is only applicable for the intermediate and heavy nuclei. However, the only necessary condition for its application is a large number of resonances at the appropriate bombarding energies, so that the cross section can be described by an average over resonances. This can in specific cases be valid for light nuclei and on the other hand not valid for intermediate mass nuclei near magic numbers. Thus another motivation of these investigations is to explore the nuclear chart for reactions with a sufficiently high level density, implying automatically that the nucleus can equilibrate in the classical compound nucleus picture.

[*] All authors equally contributed to this work.

For $Z > 50$, entering the regime of natural α decay, very small α capture Q values can be encountered for proton-rich nuclei. Such nuclei on the other hand do not play a significant role in astrophysical environments maybe with exception of p-process.

The stellar process synthesizing the heavy proton rich nuclei (the p-nuclei) is called the p-process [1]. It is generally accepted that p-process mainly involves subsequent (γ,n) reactions starting from s and r seed nuclei and driving the nuclei toward the neutron-deficient region. Along the isotopic path, the binding energies of neutrons become gradually larger. As a result, the (n,γ) and (γ,n) reactions become equilibrated, the reaction flow slows down and at some point, is deflected by (γ,α) and/or (γ,p) reactions.

The modeling of p-process nucleon-synthesis requires a large network of thousands of nuclear reactions involving stable nuclei as well as unstable, proton-rich nuclides. The relevant astrophysical reaction rates (calculated from the cross sections) are inputs to this network, and their knowledge is essential for the p-process calculations. The cross section of γ - induced reactions can be calculated from the inverse capture reactions. While there are compilations of neutron capture data along the line of stability above the iron region, there are still very few charged-particle cross sections determined experimentally, despite big experimental efforts in recent years. Thus, the p-process rates involving charged projectiles are still based mainly on (largely untested) theoretical cross sections obtained from modern Hausser-Feshbach statistical calculations.

In the case of (p,γ) reactions the models are able to reproduce the experimental data within about a factor of two and the predictions are not very dependent on the input parameters (*e.g.* optical potentials) [2] .

The existing cross section databases of (α, γ) and (p,γ), reactions relevant to the p-process, networks were built up mostly during the last years. Predominantly (p,γ) reactions were studied, because of higher expected cross sections. Different experimental methods were used for the (p,γ) studies, for example, in-beam gamma spectrometry detecting the individual transitions with angular distributions [3], summing spectroscopy using 4π scintillator setups [4] and the activation method [2, 5].

In this paper we report, briefly, on the in-beam angle-integrated cross section measurements carried out using the low background spectrometer based on the 4π NaI(Tl) summing detector installed at the 8 MV Van der Graaf Tandem of NIPNE-HH Bucharest.

One of very interesting nucleus for p-process is the odd-odd ^{138}La nucleus situated very nearly the $N = 82$ closed shell. The origin of the rare nuclide ^{138}La (9% abundance) remains one of the key questions that nucleon-synthesis theory is still trying to answer. However, ^{138}La is under produced in all p-process calculations performed so far [1, 7]; the thermonuclear origin of ^{138}La depends in a sensitive way on the competition between the ^{138}La production and the ^{138}La destruction by photo-dissociation was demonstrated very recently [8].

Therefore the primary aim of the present study is to extend the existing experimental databases to the p-process by studying the ^{139}La + p and ^{141}Pr + p systems which involve nuclei with $N = 82$. The cross sections of the ^{139}La(p, γ)^{140}Ce and ^{141}Pr (p,γ)^{142}Nd reactions were measured and the results are compared model calculations implemented with the available predictions of statistical model NON-SMOKER code [9].

2. EXPERIMENTAL EQUIPMENT AND PROCEDURES

2.1. SETUP AND TARGETS

The experiments were carried out at the 8 MV Van de Graaf Tandem of NIPNE-HH Bucharest. The ^{139}La (p,γ)^{140}Ce (Q = 8.14 MeV) and ^{141}Pr (p,γ)^{142}Nd (Q = 7.22 MeV) reactions were measured over a range of incident proton energies from 2.0 to 5.0 MeV. The incident proton energies were varied in 500 keV steps with a typical beam current on target of 10–50 nA. In order to keep the dead time below 10%, especially at $E_P \geq 3.0$ MeV, it was needed to perform data acquisition with beam currents of less than 10 nA.

The beam stop targets with thickness of 100–400 μg/cm^{2}onto 50 μ thick tantalum backings were prepared by evaporating of lanthanum and praseodymium oxides using the laser abrasion procedure leading to their decomposition and transforming in metallic targets confirmed by standard colors. The targets were checked frequently and were found to be stable during the course of experiment. The experimental setup is shown in Fig. 1.

A minimum amount of material was used in the construction of target chamber and target holder in order to reduce absorption of Γ-rays. The beam collimating system consists from two collimators on which the proton beam passes through them and is focused onto a spot of about 3 mm diameter. The distance of the target from the first and second collimator was 50 cm and 45 cm, respectively. The first collimator is a Ta plate with a hole of 3mm diameter whereas the second Ta plate (anti-scattering) has an Ø4 mm hole. The target holder is placed at the end of the stainless steel tube that was sealed with a Plexiglas plug of cylindrical shape. The target is situated in front of the Plexiglas plug and a Ta rectangular Faraday cup (20×20×20 mm) collecting the proton beam charge. A guard ring with a rectangular whole (20×20 mm) is connected at negative voltage. The target, the Faraday cup, the guard ring and the collimators are electrically insulated from the beam line with Plexiglas mounting devices. During all experiments a voltage of –300 V was applied in the guard ring in order to suppress the secondary electrons escaping from the Faraday cup at steep angles and to prevent the electrons carried

by the beam from reaching the target. The integrated beam current incident upon the Faraday cup was measured at regular intervals to determine its degree of variation during the irradiation. Its value was stable to within 3% over the duration of each irradiation. Current measurements taken from these confirmed an excellent beam quality. The pressure in tube of the target was about 1×10^{-6} Torr.

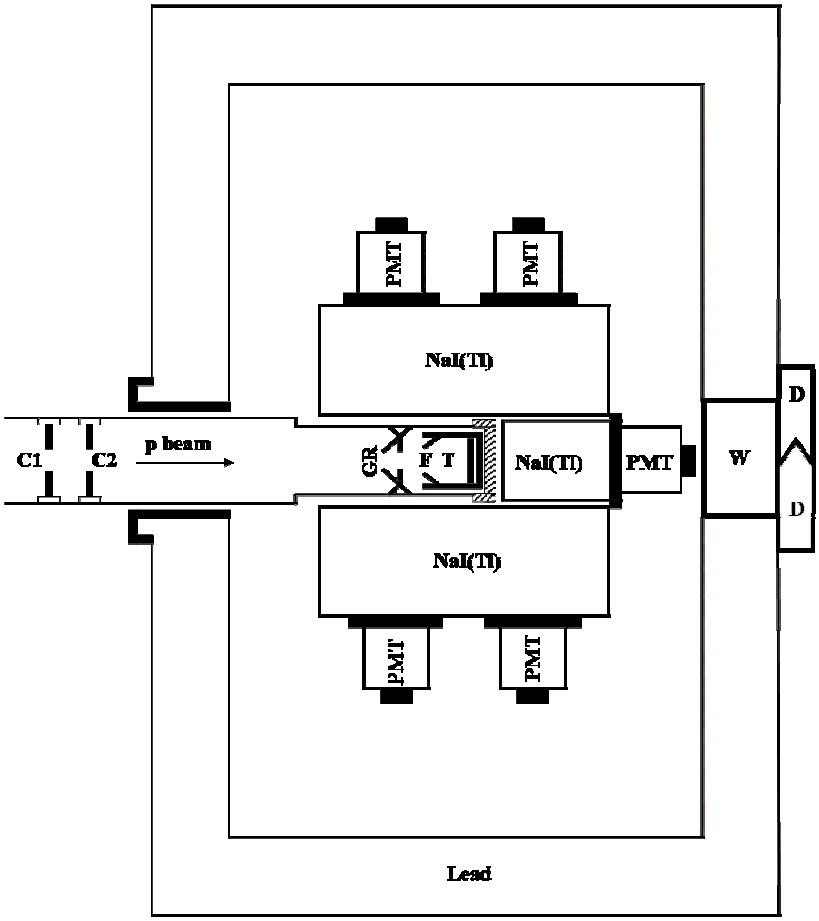

Fig. 1 – Schematic cross-section drawing of the low-background spectrometer and the beam collimating system and target supporting. Legend: C1, C2 Collimators, GR Guard ring, F Faraday cup, T Target, W Detachable lead shielding, DD Closing lead doors.

2.2. LOW-BACKGROUND SPECTROMETER USING NaI(Tl) DETECTORS

The search of very rare nuclear events, such as high energy gamma-rays resulted from proton capture reactions ask for a detection system having the lowest possible limit of detection. This latter depends mainly on its background, *e.g.* on

the signal observed in absence of the event to be detected. It is thus important to keep the background as low as achievable. When the source activity is small, it is needed to shield the spectrometer from the natural radioactive background originating from cosmic rays, the uranium and thorium series and ^{40}K. Therefore, it is important to understand the nature of the Γ-ray background in detector spectra and to investigate possibilities for reducing the background further. In order to obtain further improvement it is necessary to identify the background contribution from each remaining source and find means to eliminate it.

In the case of sodium iodide detectors this background is due to:

– radioactive materials in the detector,

– radioactivity from shielding the materials and the hardware within the shields,

– radioactive penetration of the shields from outside,

– radon inside the shields,

– effects due to the cosmic radiation.

A special attention is paid by the suppliers to reduce the intrinsic detector activity. So, the standard materials would be aluminum for housing and Pyrex glass for the windows and standard PMTs. Because of the applications, these detectors are used in often required low intrinsic detector activity, special materials can be chosen such as stainless steel or OFHC cooper for the housing, quartz windows and PMTs selected for low ^{40}K (a typical contaminant in the PMTs glass envelope).

Most of the natural background spectrum observed by a spectrometer originates from the uranium and thorium series and from ^{40}K. These radioactive elements are from almost every material in our environment in a typical 20 μR/h and integrated count rate of 100 c/s for the energy range 50 to 3 000 keV. A shield surrounding the detector can therefore remove a large fraction of the background, this rendering the contribution to other components relative more important. A 100 mm Pb shield will reduce the above count rate to less 1 c/s. Because that the NaI spectrometers are most efficient at low energies and because the shield material will convert high energy photons to lower energies by Compton scattering and pair production. The count rate reduction factor due to the shield depends on spectrometer size and radiation energy. In general, the individual spectrum lines at energies below 1MeV are attenuated by many factors than the continuum while at higher energies (1 to 5 MeV) corresponding to the absorption minimum in materials, the lines and continuum are reduced by similar amounts. The full effect of a shield in reducing the natural background is almost never realized because of shield cracks and the ducts necessary to operate a spectrometer inside.

The Radon noble gas is a decay product and together with its daughters can contribute to the activity inside a shield. To reduce the radon source, the shield needs flushing with the radon free gas after sealing. The radon activity varies with ventilation and weather.

Cosmic radiation consists of a nucleonic component, a soft component consisting mainly of photons and electrons and a hard muon component [32]. The soft component is reduced by a small amount of 100 mm lead shielding. The

nucleonic component is only a few percent of the total. The lead shield has a small effect on this component; 0.20m of concrete reduces it of 16 times. A 100 mm lead shield reduces the hard component very little. The average muon intensity at sea level is 120 / m^2s [33]. The muons can also interact with the shield and detector materials to produce thermal neutrons and activated isotopes. The large effect is seen from lead spallation neutrons. An iron shield generates fewer neutrons but needs to be more massive to achieve the same shielding factor for natural background.

Fluorescent X-rays are generated by the interaction of cosmic rays and natural radiation with shield and the detector assembly. The main lead KX-ray series lies between 72 and 82 keV, while those of iron are at 6.40 keV and 7.06 keV. The standard method of reduction is to use a graded shield linear composed of materials of successively lower atomic number. This method is however not effective for muonic X -rays (6 000 keV for lead, 1 260 keV for iron). Fortunately, the intensity of these is low. Several methods with large anticoincidence shields have been used to minimise cosmic-ray effects and reduce Compton interference. Possible sources of Γ-ray background are extensively discussed in Refs. [6].

These aspects were taken in account to design a low-background spectrometer for measuring singles gamma-ray spectra resulted from proton capture reactions.

The gamma-ray spectra were measured using the low-background spectrometer based on the large 4π NaI(Tl) summing detector installed on the beam line (Fig. 1). The summing detector is placed inside of a lead rectangular castle (85 cm × 56 cm × 55 cm) as passive shielding with lateral thickness of 7.5 cm lead; the lead walls situated above and below the NaI detectors have at an increased thickness at 10cm of lead in order to reduce the cosmic background. The chamber of castle is lined with graded linear shield of 6 mm Cooper and 2 mm Al for reducing the fluorescent X-rays produced by cosmic rays in castle materials, especially on lead passive shielding (Figs. 2–4).

This detector consists of a 12 inch × 12 inch NaI(Tl) (9HSW9/(8) 3AL BICRON) mono-crystal of cylindrical shape with a radial through hole (Ø=83mm) coinciding with the beam axis. This detector consists of two scintillation crystals of cylindrical shape; each crystal is segmented into four optically separated sections, each viewed by a photomultiplier tube. An extra 3inch ×3inch NaI(Tl) is placed behind the target, closing the through hole of the annulus detector as sketched in Fig. 1.

The 3 segmented NaI(Tl) was used as a single detector with the photomultiplier signals connected in parallel. The summed signal was passed through a spectroscopic preamplifier homemade and after gain matched, continues passing through a spectroscopic amplifier with a shaping time of 4μs, enters into ADC module. The target is placed at the centre of the crystal, which covers a solid angle of 98%.

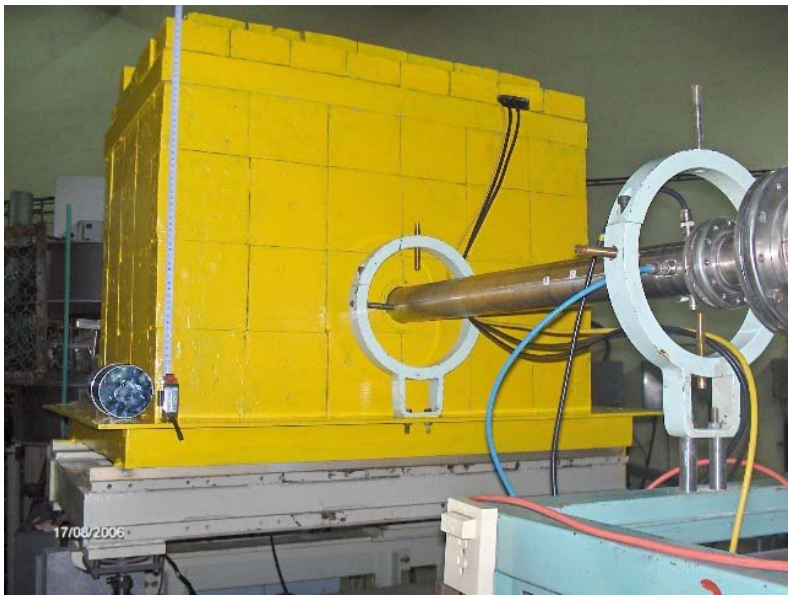

Fig. 2 – Front view of the low-background spectrometer.

Fig. 3 – Back view of the low-background spectrometer showing the 4π NaI(Tl) summing detector and the plexiglass plug for target supporting.

Fig. 4 – Back view of the low-background spectrometer showing the Ge(Li) measuring the background inside of lead castle.

The main advantage of using such a *summing* detector is that the response of the NaI(Tl) crystal leads predominantly to a single peak called *sum peak,* at the sum of the energies of the cascading transitions, *i.e.* at $E^{\gamma} = Q + E_{cm}$, where Q is the Q-value of the reaction and E_{cm} is the center-of-mass projectile energy. Due to the almost 4π geometry covered by the detector, angle-integrated γ fluxes can be measured. Thus, corrections for angular distribution effects are not necessary. The "ideal" picture of having just one peak is not achieved in "real" experiments where the spectra also include some Compton continuum, since some photons escape from the NaI(Tl) crystal mainly through its borehole and also other photons are coming from cosmic background not completely suppressed by the castle shielding.

Finally, the background in spectrometer can be substantially reduced but the presence of cosmic background remains to be taken in consideration in the data processing. As is shown in the summed background spectrum (Fig. 5) proves that the shield material converts high energy photons to lower energies by Compton scattering and pair production. The first preeminent peak of 1 260 keV is due to the fluorescent muonic X-rays produced in the structural iron materials by muons from cosmic rays.

The γ-single spectra measured with the summing detector include not only γ rays from our reactions, but also Γ rays arising from the Ta backing as well as cosmic background above mentioned (Figs. 6, 7). The spectra were subtracted for backings and cosmic residual background resulting thus difference spectra.

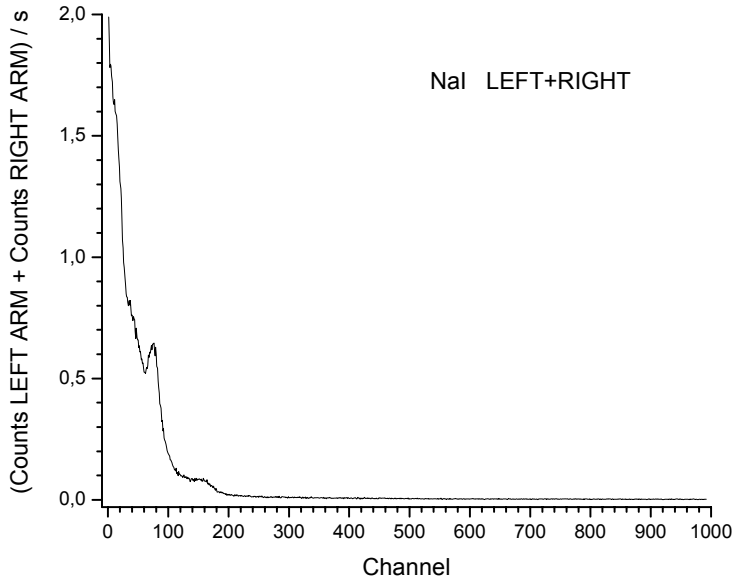

Fig. 5 – Experimental energy spectrum deposited by cosmic muons in the two arms of the 4π NaI(Tl) summing detector. The preeminent peak viewed in spectrum is due to muonic X-ray of Iron (1 260 keV).

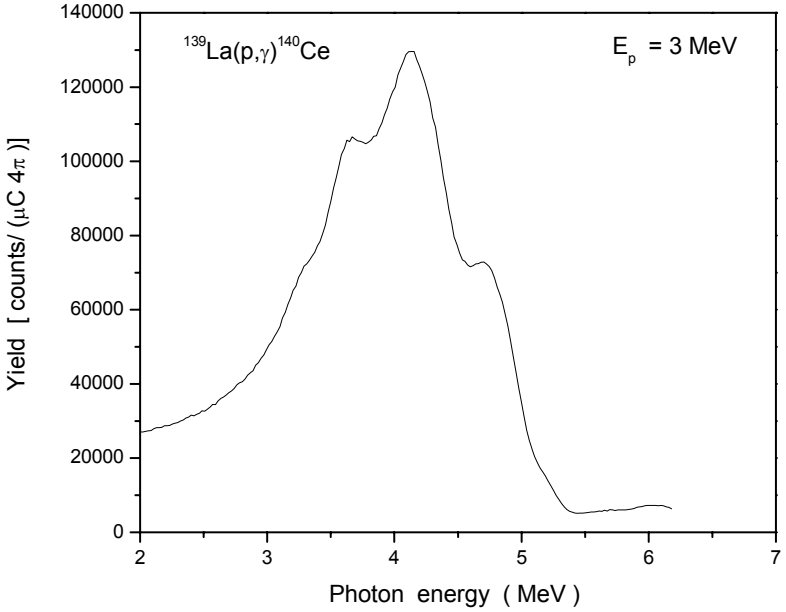

Fig. 6 – Gamma-ray spectrum measured at E_p = 3 MeV for Lanthanum target. The results of the present work have been derived from the analysis of difference spectra.

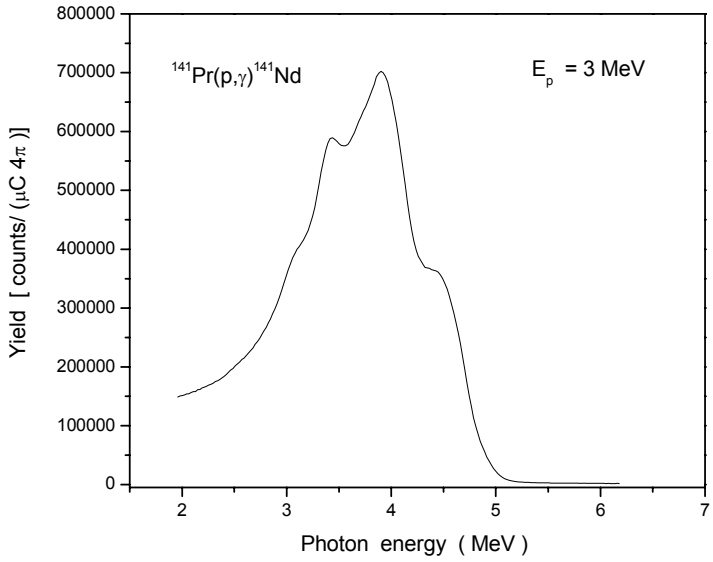

Fig. 7 – Gamma-ray spectrum measured at E_p = 3 MeV for Praseodymium target. The results of the present work have been derived from the analysis of difference spectra.

3. DATA ANALYSIS AND RESULTS

When the ^{140}Ce and ^{142}Nd nuclei are excited in the (p,γ) reactions, the absolute yield of all the γ transitions feeding their ground state are derived and thus have to be measured. The excited states of above mentioned nuclei can be populated by γ transitions de-exciting higher lying discrete levels (*secondary γ rays* or *cascade feeding*) as well as entry state (*primary Γ rays* or *direct feeding*). The entry state has an excitation energy of $E_X = Q + E_{cm}$, so more γ_0 transitions to ground state can be present in spectra. At such high excitation energies ($E_X \geq Q$ = 8.14 MeV and 5.226 MeV for ^{140}Ce and ^{142}Nd nuclei, respectively) the level densities of the produced compound nucleus is very high, i.e., the average spacing between the excited levels are less than some hundred of eV. Due to the thickness of target (tens of keV) and the beam energy spread is much smaller (1-3keV), the γ_0 transition is the result of the decay of all entry states populated by reactions to the ground states.

In order to obtain the total cross section σ_T, the absolute yield Y_0, i.e., the absolute number of all photons emitted by the ^{139}La(p,γ)^{140}Ce and ^{141}Pr(p,γ)^{142}Nd reactions, has to be determined.

The absolute yield Y_0 is given by:

$$Y_0 = \frac{\Phi}{Q} \cdot \frac{1}{s}, \tag{1}$$

where Φ is the angle-integrated Γ-ray flux measured at energy E, Q is the corresponding accumulated charge and **ε** is absolute efficiency of the detector. The experimental yields $Y_{exp} = \Phi / Q$ were obtained from the "difference" spectra described in Section II, whereas the absolute efficiency ε was obtained by the procedure described in the following.

The absolute efficiency **ε** of summing detector has been determined with the radioactive sources (^{133}Ba, ^{137}Cs, ^{60}Co, ^{152}Eu and ^{56}Co) as by means of the reactions investigated as followings: ^{27}Al(p,γ)^{30}Si at E_p = 2.0 MeV, ^{10}B(p,γ)^{11}C and ^{39}K(p,γ)^{40}Ca at E_p = 2.2 MeV. These reactions provide γ rays of up to 11.7 MeV with very well known intensities, from resonances that have been extensively investigated. The corresponding absolute efficiencies **ε** has been used to obtain the absolute yields defined in Eq. (1). A correction was applied to experimental yields due to presence of ^{138}La in the natural composition of Lanthanum.

The total cross section σ_T is obtained from

$$\sigma_T = Y_0 \frac{A}{A_n} \cdot \frac{1}{\xi}, \tag{2}$$

where A is the atomic weight of the target in a.m.u., N_A is the Avogadro number, and ξ is the target thickness. The resulting total cross sections σ_T at the center-of-mass energy are given for the two reactions are given in Table 1. The total errors in cross sections given in Table 1 are the order of 9–12 % except for those of in the lowest energies being in the range of 15–20 %.

Table 1

Total cross sections (σ_T) of ^{139}La(p,γ)^{140}Ce (a) and ^{141}Pr (p,γ) ^{142}Nd (b) reactions measured in the present work, where E_{cm} is the center-of-mass energy

E^{cm} [MeV]	σ_T [nb] (a)	σ_T [nb] (b)
1.985	4±1	2.20±0.04
2.482	82±13	27±5
2.978	240±35	512±61
3.474	3648±391	15820±1742
3.971	8724±862	85325±8533
4.467	17563±1754	165832±16586
4.964	37427±3370	253416±22807

The total cross sections σ_T at the center-of-mass energy can be used for calculations of the corresponding astrophysical S factors by

$$S(E) = \sigma_T (E)\, E\, e^{2\pi\eta}, \tag{3}$$

where η is the Sommerfeld parameter [11] defined by

$$2\pi\eta = 31.29 Z_1 Z_2 \left(\frac{\mu}{E}\right)^{1/2}. \tag{4}$$

In the last equation, the reduced mass μ is in a.m.u. and the center-of-mass E is in units of keV, so that S factor are in keV.

The energies given in the first column of Table 1are effective energies in the center-of-mass system. They were determined by using appropriate stopping powers [12] by:

$$E_{eff} = E_p - \frac{\Delta E_Y}{2}. \tag{5}$$

where E_p is the beam energy and ΔE_Y are the energy losses in the target material.

4. DISCUSSION

The main goal of the present work is to investigate the validity of the different nuclear parameters of the Hauser-Feshbach (HF) calculations. In the HF theory, the cross section for the decay of a compound nucleus into one of the exit channels is given by:

$$\sigma_{\alpha\beta} = \pi\lambda_\alpha^2 \frac{1}{(2I+1)(2i+1)} \sum J^\pi (2J+1) \frac{T_\alpha^{J^\pi} T_\beta^{J^\pi}}{\sum_\alpha T_\alpha^\pi}, , \tag{6}$$

where α, β denote the entrance and exit channels respectively, and I, i are the target and projectile spins, respectively. $T_\beta^{j\pi}$ are the transmission coefficients summed over all orbital and channels spins to give the total transmission coefficient for the formation of the compound nucleus in the state J^π. When the compound nucleus is excited to state in the continuum, the transmission coefficients in Eq.(6) are averaged over a specified nuclear level density. For example, the denominator in Eq. (6) is given by:

$$\sum_\alpha T_\alpha^{J^\pi} = \sum_\alpha{}' T_\alpha^{J^\pi} + \sum_{I\alpha} \int \omega_1 (U) T_\alpha^{J^\pi} E_\alpha \mathrm{d}E_\alpha, \tag{7}$$

where ω_I (U) is the density of levels of spin I in the residual nucleus. The Σ' indicates that the sum is taken over only those channels leading to the first few discrete levels in the residual nucleus; all other channels are included in the integrals over the excitation energy E_α of the residual nucleus.

Apart from the Q values of the decay channels, the other main nuclear properties, the HF cross section depends on the transmission coefficients for particle and the nuclear level densities of the compound and residual nuclei in different decay channels. For the sake of nucleon-synthesis applications, one needs to develop global models that would enable the evaluation of these properties for the thousands of nuclei and nuclear reactions involved in a most reliable way. For this purpose, there exist global phenomenological models of nuclear level densities

based on the Fermi gas model description of the excited nucleus, and also microscopic models based on single-particle spectra associated with realistic effective potentials. The main advantages of these models is that they take in account the discrete structure of the nucleus and treat shell, pairing and deformation effects consistently, whereas the former models consider these effects by means of empirical corrections

In the present work, the calculations of the HF cross sections are carried out with the statistical model NON-SMOKER [9], due to the fact that the MOST code was unavailable [10]. The NON-SMOKER code based on the well-known SMOKER code [14], an improved code for the prediction of astrophysical cross sections and reaction rates in the statistical model has been developed. The current status of the new NON-SMOKER code is described in the following.

The final quantities entering in the expression for the cross section in the statistical model [13] are the averaged transmission coefficients. They do not reflect a resonance behavior but rather describe absorption via an imaginary part in the (optical) nucleon–nucleus potential [15]. In astrophysics, usually reactions induced by light projectiles (neutrons, protons, α-particles) are most important. Global optical potentials are quite well defined for neutrons and protons. It was shown [14, 16, 17] that the best fit of s–wave neutron strength functions is obtained with the optical potential by [19], based on microscopic infinite nuclear matter calculations for a given density, applied with a local density approximation. It includes corrections of the imaginary part [20, 21]. A similar description is used for protons. Optical potentials for α - particles are treated in the folding approach [22], with a parameterised mass- and energy-dependence of the real volume integral [23]. The mass- and energy-dependence of the imaginary potential is parameterised according to [24] and additionally includes microscopic and deformation information [23]. Deformed nuclei are treated by an effective spherical potential of equal volume [15, 18]. For a detailed description of the formalism used to calculate E1 and M1 γ transmission coefficients and the inclusion of width fluctuation corrections [25], see [14] and references therein.

The level density treatment has been recently improved [19]. However, the problem of the parity distribution at low energies remained. The new code includes a modified version of the description [14], accounting for non-evenly distributed parities at low energies, based on most recent findings within the framework of the shell model Monte-Carlo method [26].

Additionally, the included data set of experimental level information (excitation energies, spins, parities) has been updated [27], as well as the experimental nuclear masses [16]. These data bases are continuously updated. For theoretical masses, there is a choice between different mass models (*e.g.* by Hilf *et al.* [28], FRDM [29], ETFSI [30]), of which currently the FRDM is favored. Microscopic information needed for the calculation of level densities and α + nucleus potentials are also taken from the FRDM, as well as experimentally

unknown ground state spins [31]. Finally, isobaric analog states $T> = T< + 1 =$ Tg.s. + 1 are explicitly considered in the new code (the Gamow window) in the calculation of the rates.

The code NON-SMOKER allows one to study isospin effects due to incomplete isospin mixing in the nuclear states. Standard Hauser-Feshbach calculations usually neglect isospin which is equivalent to assuming completely isospin-mixed states. Incomplete isospin mixing leads to a suppression of the neutron channel in proton-induced and thus to an enhancement of the (p,γ) cross section above the (p,n) threshold, compared to calculations with complete isospin mixing may appear when the first isobaric analog state in compound nucleus is above or closely below the neutron threshold of the compound nucleus.

More data are needed which cover a large energy interval above and below the (p,n) threshold, as the application of width fluctuation corrections also has an impact on the cross sections below the threshold.

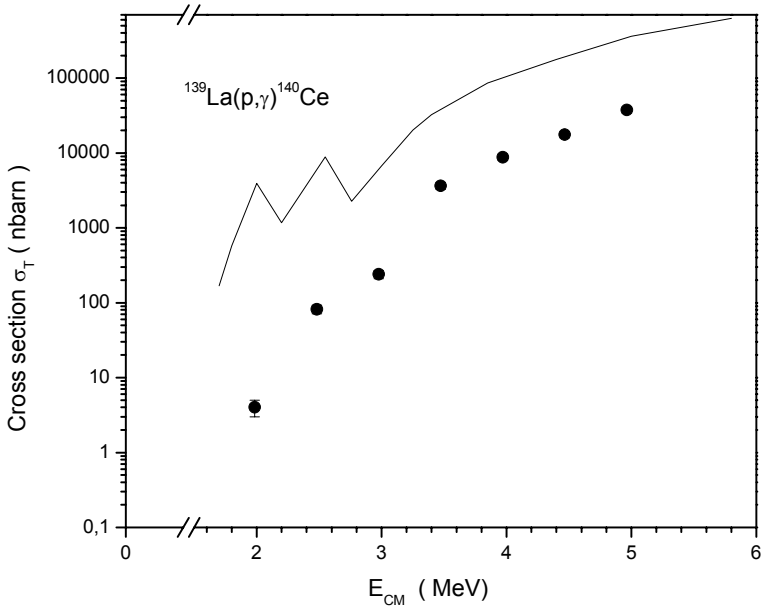

Fig. 8 – Comparison of the cross sections (solid circles) measured for ^{139}La(p,γ)^{140}Ce reaction in the present work with the predictions of Hausser-Feshbach theory (curve) calculated with the code NON-SMOKER [9].

The final analysis of the measured data is in progress. Figures 8 and 9 show the preliminary result with some of the measured points. The solid curves in the figures are the statistical model calculation of the NON SMOKER code using standard parameter set [9]. At this early stage of the data analysis it seems that the theory overestimates the measured data.

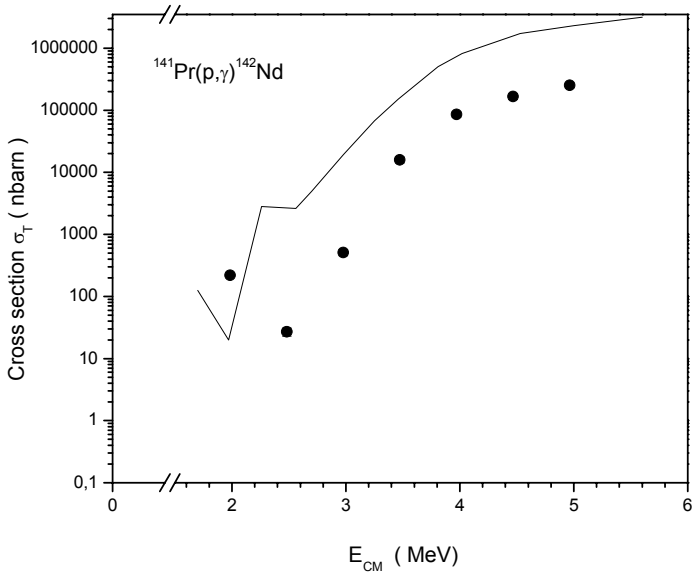

Fig. 9 – Comparison of the cross sections (solid circles) measured for ^{141}Pr (p,γ) ^{142} Nd reaction in the present work with the predictions of Hausser-Feshbach theory (curve) calculated with the code NON-SMOKER [9].

5. CONCLUSIONS

The cross sections of the ^{139}La(p,γ)^{140}Ce and ^{141}Pr (p,γ)^{142}Nd reactions were measured at E_p=2–5 MeV in steps of 0.5 MeV and were found with relative errors decreasing from 20 down to 9% with increasing beam energy. These cross sections resulting from the analysis of a part of the data which will be extended by next measurements by means of in-beam gamma spectrometry detecting the individual transitions with a Germanium detector coupled with the present 4π NaI summing detector used as Compton suppressor.

Thus, the very precise data will allow a distinct determination of cross sections and their final analysis of deduced astrophysical *S*-factors and reaction rates can be used as to test the applicability of statistical models within p-process simulations. At this early stage of the data analysis it seems that the predictions of the statistical model code NON-SMOKER overestimate the experimental data.

In conclusion, the code NON-SMOKER makes use of the latest set of descriptions for the calculation of the nuclear properties needed to reliably predict astrophysical reaction rates, such as masses, level densities, nucleon- and α-potentials, GDR energies and widths, width fluctuation corrections, additionally, the possibility of studying isospin.

Nevertheless, more experimental data are needed to check and further improve current parameterisations. Especially investigations over a large mass range would prove useful to fill in gaps in the knowledge of the nuclear structure of many isotopes and to construct more powerful parameter systematic. Such investigations should include neutron-, proton- and α-strength functions, as well as radiative widths, and charged particle scattering and reaction cross sections for stable and unstable isotopes.

The results of the present work suggest further cross-section measurement of (p,γ) reactions in the $N = 82$ mass region, in order to derive the systematic needed for a globalization of the nuclear HF calculations.

REFERENCES

1. M. Arnould and Goriely, Phys. Rep., **384**, 1 (2003).
2. Gy. Gyurky et al., Phys. Rev., **C68**, 055803 (2003).
3. S. Galanopoulos et al., Phys. Rev., **C67**, 015801 (2003).
4. P. Tsagari et al., Phys. Rev., **C70**, 015802 (2003).
5. Gy. Gyurky et al., Phys. Rev., **C64**, 065803 (2001).
6. G.Heusser, Ann. Rev.Nucl. Part. Sci, **45**, 543 (1995).
7. S. Goriely et al., Astron.Astrophys., **375**, L35 (2001).
8. H.Utsunomiya et al., Phys. Rev., **C74**, 025806 (2006).
9. T. Rauscher, F. K. Thielemann and K. L. Kratz, Phys. Rev., **C56**, 1613 (1997).
10. S. Goriely, in S. Wender (Ed.), Proc. *Capture Gamma-Ray Spectroscopy and Related Topics,* IOP Conference Proceedings, Vol. 529, 2000, p. 287.
11. E. Rolfs and W.S. C. Rodney, *Cauldrons in the Cosmos*, The University of Chicago Press, Chicago Press, Chicago, 1988.
12. J. F. Ziegler and J.P. Biersack, *Code SRIM, version 2000.39*, Full description given by J. F. Ziegler, J.P. Biersack and U.Littmark, in *The Stopping and Range of Ions in Solids*, Pergamon, New York, 1985.
13. W. Hausser and H. Feshbach, Phys. Rev., **87**, 366 (1952).
14. F. K. Thielemann, M. Arnould and J.W. Truran, in *Advances in Nuclear Astrophysics,* edited by E. Vangioni-Flam, J.Audouze, M. Casse, J.P. Chieze and J. Tran Thanh Van, Editions Frontieres, Gif-Sur-Yvette, 1986, p. 525.
15. C. Mahaux and H. A. Weidenmuller, Ann. Rev. Part. Nucl. Sci., **29**, 1 (1979).
16. F.K. Thielemann, J. Metzinger and H. V. Klapdor, Z. Phys., **A 309**, 30 (1983).
17. J. J. Cowan, F. K.Thielemann and J. W. Truran, Phys. Rep., **208**, 267 (1991).
18. J. P. Jeukenne, A. Lejeune and C. Mahaux, Phys. Rev., **C 16**, 804 (1977).
19. S. Fantoni, B. L. Friman and V. R. Pandharipande, Phys. Rev. Lett., **48**, 1089 (1981).
20. C. Mahaux, Phys. Rev., **C 82**, 1848 (1982).
21. G. R. Satchler and W. G. Love, Phys. Rep., **55**, 183 (1979).
22. T.Rauscher, Proc. Int. Workshop XXVI on *Gross Properties of Nuclei and Nuclear Excitations*, Hirschegg , eds. J. Wambach *et al.*, Darmstadt Gesellschaft fur Schwerionenforschung, 1998.
23. Brown G E and Rho M, 1981 Nucl. Phys., **A372**, 397 (1981).
24. J. W. Tepel, H. M. Hofmann and H. A. Weidenmuller, Phys. Lett., **49B**, 1 (1974).

25. H. Nakada and A. Alhassid, Phys. Rev. Lett., **79**, 2939 (1997).
26. *** Database ENSDF, NNDC, Brookhaven National Laboratory, Upton, USA.
27. G. Audi and A. H. Wapstra, Nucl. Phys., **A595**, 409 (1995).
28. E. H. Hilf, H. von Groote H and K. Takahashi, Proc. Third Int. Conf. on *Nuclei far from Stability*, Geneva, CERN 76-13, 1976, p 142.
29. P. Moller, J.R Nix, W.D. Myers, and W. J. Swiatecki, At. Data Nucl. Data Tables, **59**, 185 (1995).
30. Y. Aboussir, J. M. Pearson, A. K. Dutta, and F. Tondeur, At. Data Nucl. Data Tables, **61**, 127 (1995).
31. P. Moller, J.R. Nix J and K. L. Kratz, At. Data Nucl. Data Tables, **66**, 131 (1997).
32. B. Mitrica et al., Rom. Rep. in Phys., **62**, *4*, 750–757 (2010).
33. B. Mitrica, AIP Conf.Proc., **972**, 500–504 (2008).